

Experiments on the Dynamic Behavior of Cavitating Pumps

S. L. NG¹

C. BRENNEN

California Institute of Technology
Pasadena, Calif.

This paper describes experiments performed to measure the dynamic transfer matrices for cavitating (and noncavitating) pumps. These transfer matrices describe the relationship between small linear oscillatory perturbations in the pressures and mass flow rates at inlet and discharge from the hydraulic machine. The matrices were deduced from direct measurements of these fluctuating quantities for different modes of excitation of the machine. Results for a cavitating inducer are presented as functions of frequency and mean operating state. Though some of the trends in the data are consistent with existing theoretical models of inducer dynamics, others are not, indicating a need for further theoretical investigation of the dynamic characteristics of such flows. The results exhibit increasingly complex dynamics with increasing cavitation; it appears that the hydraulic machine deviates from an essentially passive response without cavitation to an increasingly active response as the cavitation number is reduced.

1 Introduction

The ubiquity of pumps and turbines and the rapidly expanding need to analyze the transient behavior and stability of the hydraulic systems of which they are a part has created renewed demands for knowledge of the *dynamic* performance of hydraulic machines (see, for example [3], [6], [8]).² Typically such need has arisen either because of unexpected system instabilities (e.g. [29], [25]) or because of demands for more accurate analytical tools for the prediction of known instabilities (e.g. [24], [31], [28]) or transients ([18], [17], [11]). This paper is confined to dynamic phenomena of relatively low frequency which are hydrodynamic rather than purely acoustical; such frequencies are typically of the order of tens of Hertz or less. In many hydraulic systems the instabilities causing greatest danger to the integrity of the system lie within this description.

Within this frequency range, a major stumbling block to further understanding of the dynamics of hydraulic systems is the lack of knowledge of the relations between the unsteady pressures and mass flow rates at inlet to a hydraulic machine and the same quantities at discharge. The present experiments were intended to determine these relations for several axial inducers. The investigations concentrate on the relations for small amplitude, linear perturbations of the mean flow. Clearly one must understand this simpler case before proceeding to

large amplitude oscillations which are likely to involve significant nonlinearities for most hydraulic machines. Furthermore, fluctuations in the shaft speed of the machine are neglected; the present experiments were typical of many turbomachines in the sense that the large inertia of the prime-mover, gear box, and impeller inhibits any significant shaft speed fluctuation.

Consider a single fluctuation frequency, Ω . The small linear perturbations in total pressure at inlet and discharge will be denoted by the real parts of $\tilde{h}_1^* e^{i\Omega t}$ and $\tilde{h}_2^* e^{i\Omega t}$, respectively; the mass flow rates will be denoted by the real parts of $\tilde{m}_1^* e^{i\Omega t}$ and $\tilde{m}_2^* e^{i\Omega t}$. The quantities \tilde{h}_i^* , \tilde{m}_i^* are complex in order to denote the relative phases of the various fluctuations. It is convenient to nondimensionalize these quantities by defining

$$\tilde{h}_i = \tilde{h}_i^* / \frac{1}{2} \rho U_T^2 \quad ; \quad m_i = m_i^* / \rho U_T A_{11} \quad (1)$$

Thus the desired relations between the fluctuating total pressure and mass flow rates at inlet and discharge can be described by a transfer matrix $[ZP]$ defined as

$$\begin{Bmatrix} \tilde{h}_2 - \tilde{h}_1 \\ \tilde{m}_2 - \tilde{m}_1 \end{Bmatrix} = \begin{bmatrix} ZP_{11} & ZP_{12} \\ ZP_{21} & ZP_{22} \end{bmatrix} \begin{Bmatrix} \tilde{h}_1 \\ \tilde{m}_1 \end{Bmatrix} \quad (2)$$

The transfer matrix, $[ZP]$, will be a function not only of frequency, Ω , but also of the mean operating state of the machine. The former is represented by a nondimensional frequency, $\omega = \Omega H / U_T$. The latter is conveniently defined by either the flow coefficient, φ , or the head coefficient, ψ . In the event of cavitation an additional parameter namely the cavitation number, σ , is needed to describe the mean operating state.

A brief phenomenological and historical discussion of the transfer matrix $[ZP]$ may be valuable at this point. In the

¹Now at Chevron Oil Field Research, La Habra, Calif.

²Numbers in brackets designate References at end of paper.

Contributed by the Fluids Engineering Division for publication in the JOURNAL OF FLUIDS ENGINEERING. Manuscript received by the Fluids Engineering Division, May 31, 1977.

absence of cavitation and neglecting the compressibility of the liquid and containing structure it follows from continuity of mass that both ZP_{21} and ZP_{22} should be zero. Furthermore the total pressure rise across the pump should be independent of the absolute level of the total pressure. Consequently ZP_{11} should be zero and only the impedance term, ZP_{12} , remains unknown. Notice that under these circumstances the determinant, D , of $[ZP] + [I]$ where $[I]$ is the unit matrix becomes unity. This implies that the dynamic response of the hydraulic machine is essentially "passive" under the conditions described above. On the other hand, in the presence of cavitation all four elements of the transfer matrix become unknown and the determinant, D , may no longer be unity, implying "active" dynamic behavior for the device.

Until quite recently those faced with the need to construct dynamic transfer matrices have had little experimental or theoretical knowledge to guide them. For very low frequencies (or gradual transients) it was possible to argue that the hydraulic machine would simply traverse its steady-state performance curves (see for example [16], [30], [27]). This requires that ZP_{21} and ZP_{22} be effectively zero and results in purely real values for both ZP_{11} and ZP_{12} ; the former is clearly related to the slope of the head rise versus inlet pressure characteristic at the mean operating point; the latter is related to the slope of the head rise versus flow rate characteristic at the mean operating point and is conveniently described by a resistance R such that $ZP_{12} = -R$.

Such simple transfer functions are limited to very low frequency (though their actual range of validity could not be determined without dynamic experiments). Consequently attempts have been made to generate transfer functions for higher frequencies by incorporating first-order, quasistatic terms which are linear in frequency (see for example, [25], [27], [9], [28]). These somewhat arbitrary modifications usually consist of

(i) The addition of an inertial component to the impedance so that $ZP_{12} = -(R + j\omega L)$ where L is the inductance. This is intended to account for the pressure difference across the hydraulic machine generated by the acceleration of the mass of fluid within it.

(ii) The addition of a compliance, C , such that $ZP_{21} = -j\omega C$. Though liquid and structural compressibility within the machine could contribute to such a term, it has primarily been used to empirically account for the presence of cavitation.

The real problem is that there is very little reliable and complete experimental data which could be used to justify these models, or, at the very least to determine their range of validity in terms of the frequency at which the results diverge from quasi-steady models. As far as we can determine, the present paper represents the first time that complete four terminal testing has been performed on a hydraulic machine, in the sense

that both the inlet and discharge fluctuating pressures and mass flow rates have been measured. There have however, been previous dynamic measurements on hydraulic machines which though incomplete in the sense that both inlet and discharge mass flow rates were not measured directly do provide some useful insight. Anderson, Blade, and Stevens [3] performed such measurements on a centrifugal pump in the absence of cavitation. Though their data has substantial scatter, particularly at higher frequencies of fluctuation (up to 50 Hz) there is evidence that at lower frequencies the resistance, R , increases and the inductance, L , decreases with frequency. Clearly one could expect that the resistance would change with frequency due to the complicated behavior of the fluctuating boundary layers, separated flows and trailing vortex sheets.

As mentioned earlier, the situation becomes more difficult when the pump or turbine cavitates. There is no fundamental reason to expect that the effects of the cavitation would be confined to the compliance, C , introduced in the empirical models. Considerable effort has been made to evaluate the cavitating pump dynamics of liquid rocket engine turbopumps because of the important role played by the dynamics of these pumps in the POGO instability of liquid propelled rockets ([20], [25], [31], [19]). In the absence of direct measurements the mass flow rates in these field tests were inferred from pressure measurements using assumed dynamic models of the systems attached to the pump. Because of their lack of sensitivity such methods have not proved particularly definitive, especially with regard to ZP_{21} and ZP_{22} .

There have also been a number of theoretical efforts to evaluate the elements of cavitating inducer transfer functions. Most of these ([29], [15], [5], [6]) have been based on analyses of unsteady cavitating cascade flows in which the cavitation is in the form of fully developed blade cavities. In particular, it has been pointed out ([6]) that even in a quasi-static analysis blade cavity volumes will fluctuate with the fluctuating angle of attack as well as the fluctuating inlet pressure. This leads to a non zero value of ZP_{22} of the form $-j\omega M$ where M has been termed the mass flow gain factor. However, cavitation patterns in actual inducers are often much more complex involving bubble cavitation and tip vortex and backflow cavitation in addition to attached blade cavities. The dynamics of these other forms of cavitation have only received very limited analytical attention thus far ([4], [10]).

2 The Dynamic Pump Test Facility

The facility fabricated for the purpose of measuring the transfer functions and other dynamics characteristics of cavitating and non-cavitating axial flow pumps and inducers is shown diagrammatically in Fig. 1. A detailed description of the facility

Nomenclature

a = accelerometer measurement
 A_{11} = impeller inlet area
 A_{AA}, A_{BB} , etc. = flow areas at sections AA , BB , etc.
 C = compliance (dimensionless)
 D = determinant of $[ZP] + [I]$
 h = dimensionless total pressure, $h^* / \frac{1}{2} \rho U_T^2$
 h^* = total pressure
 H = blade tip spacing ($= 2\pi R^*/N$)
 $[I]$ = unit matrix
 j = imaginary index
 K = cavitation compliance (dimensionless)
 l_1, l_2, l_3 = specific lengths (Fig. A1)

L = inductance (dimensionless)
 \mathcal{L} = inductance (for the purposes of Appendix A this is evaluated as $\int dx/A(x)$ where $A(x)$ is the cross-sectional area of the flow as a function of axial position, x)
 m = dimensionless mass flow rate, $m^*/\rho U_T A_{11}$
 m^* = mass flow rate
 M = mass flow gain factor (dimensionless)
 N = number of impeller blades
 P = pressure
 P_v = vapor pressure
 p = dimensionless pressure, $P / \frac{1}{2} \rho U_T^2$

(Nomenclature continued on next page)

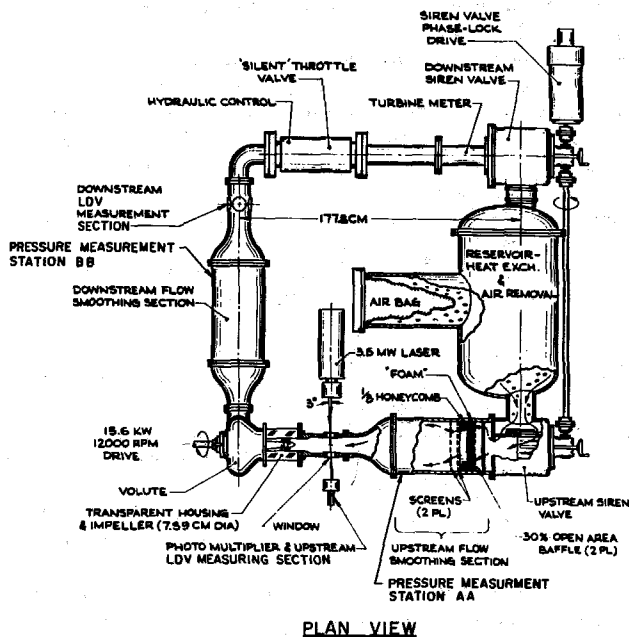


Fig. 1 Schematic plan view of the dynamic pump test facility

is given by Ng ([22]) and only the essential components are outlined here.

The mean flow generated by the pump proceeds clockwise around the circuit of Fig. 1. The mean flow rate was automatically controlled by means of a feedback system from a turbine flow meter to the hydraulically operated throttle valve (the typical response time of this system was of the order of 5 seconds so that it did not interfere with imposed fluctuations).

The basic intent of the experiments was to impose small linear fluctuations on this mean flow over a range of frequencies (up to 42 Hz) and to measure the pressure and mass flow rate fluctuations at inlet to and discharge from the pump. Preliminary feasibility studies indicated that the total inductance of the facility had to be minimized in order to achieve moderate levels of pressure fluctuation in conjunction with levels of mass flow rate fluctuation sufficiently large to be measured with reasonable accuracy. This accounts for the compactness of the facility.

Rudimentary examination of the form of the transfer function, $[ZP]$ (equation (2)) established that a single set of measurements of \bar{h}_1 , \bar{h}_2 , \bar{m}_1 , and \bar{m}_2 is insufficient to determine the matrix elements; at least two different "sets" of measurements at the same frequency and mean operating state are required. This necessitates the capability of exciting the system in a number

of modes (at least two) to obtain a number of *linearly independent* "sets" of data. In the present experiment this was accomplished using two fluctuators (see Fig. 1). By varying the relative amplitudes of these fluctuators and the phase between them, any number of linearly independent "sets" of data could be obtained for the same frequency and mean operating state. Typically we obtained three or four "sets" of data; then a least squares fitting procedure (see Appendix B) was used to solve for the transfer function, $[ZP]$.

The fluctuators basically acted like variable, oscillatory resistances at their respective positions in the circuit. Within them the flow bifurcates; one stream provides the mean component of the total flow, the other is directed through concentric slotted cylinders one of which rotates in order to generate the oscillatory component of the flow. The rotors within the two fluctuators are linked by a common shaft and are rotated at a constant speed by a phase-lock drive motor. This motor is, in turn, driven by a signal of prescribed frequency generated in a Bafco return signal analyzer. Feedback from the drive motor ensured that the excitation of the hydraulic system was phase-locked to this reference signal. This worked well up to 45 Hz. above which phase could not be maintained.

The large air bag shown in Fig. 1 essentially decouples the activities of the two fluctuators. It was also used to control the overall pressure level within the hydraulic system.

3 Fluctuating Signal Level and Measurement

The most difficult aspect of the experiment is the measurement of fluctuating mass flow rate. Within the range of excitation frequencies the measurements of fluctuating pressure were relatively simple and were made using Statham transducers at the points indicated in Figs. 1 and A1. On the other hand, the fluctuating mass flow rates were derived from measurements of the fluctuating velocities made with two laser doppler velocimeters (LDVs). Special sections fitted with lucite windows, one upstream and the other downstream of the pump (Fig. 1) permitted measurement of the instantaneous velocities in the centers of those sections. Three major design and measurement considerations were involved in the use of these LDVs:

(i) The amplitude of the imposed mass flow fluctuations had to be sufficiently large so that they could be measured with accuracy but small enough to lie within a regime of linear perturbation. Several tests were carried out to investigate the linearity of the system at various levels of excitation ([22]). The simplest of these involved tests with only one fluctuator activated; as the fluctuation amplitude was increased the response of the system was observed to be linear up to and beyond amplitudes of mass flow rate fluctuation of the order of about 2 percent of the mean mass flow rate. Other tests, including the "third-harmonic test" discussed in Section 6, resulted in this level of fluctuation

Nomenclature (continued)

R = resistance (dimensionless)	
R^* = impeller tip radius	
t = time	
U_A = mean axial fluid velocity at impeller inlet	
U_T = impeller tip speed	
v = axial fluid velocity	
$[Z]$ = overall dynamic transfer matrix	
$[ZP]$ = pump transfer matrix	
ρ = liquid density	
σ = cavitation number = $(\bar{P}_1 - P_v) / \frac{1}{2}\rho U_T^2$	
ϕ = flow coefficient, U_A/U_T	
ψ = head coefficient, $(\bar{h}_2^* - \bar{h}_1^*)/\rho U_T^2$	

Ω = fluctuation frequency
ω = reduced frequency, $\Omega H/U_T$

Subscripts

i = designating inlet ($i = 1$) or discharge ($i = 2$) quantities
M_i = measured fluctuating quantities
N_i = fluctuating quantities corrected for acceleration effects

Superscript

$\bar{}$ = overbar denotes mean, time-averaged quantity
\sim = tilde denotes complex, fluctuating quantity
n = designates an individual experimental measurement

being used in all of the transfer function measurements. The corresponding amplitude of pressure oscillation was of the order of $2.5 \times 10^4 \text{ N/m}^2$ compared with the typical total pressure rise across the impeller of $7 \times 10^5 \text{ N/m}^2$. However, it should be pointed out that this comparison of the pressure amplitude could lead to a somewhat false sense of security when dealing with cavitating flows in which the local absolute pressure in the cavitating region becomes very much smaller than the head rise. Inevitably the percentage fluctuation in the cavitation number becomes larger and larger as the mean cavitation number is reduced (see Section 6).

(ii) The point velocity measurements made by the LDVs had to be accurate manifestations of the instantaneous mass flow rates and the level of turbulence in the measurement sections (picked up as noise by the LDVs) had to be sufficiently small to achieve acceptable fluctuating signal to noise levels. Toward these ends the flow prior to each LDV measuring section is smoothed by means of screens and honeycombs followed by carefully designed nozzles of 9:1 contraction ratio (see Fig. 1). The need to do this downstream of the pump because of the highly turbulent pump discharge exacted a price: the downstream smoothing section had its own dynamic characteristics which had to be determined and subtracted from the measured transfer function in order to extract the transfer function of the pump alone (see Appendix A). As a result of these devices the turbulence level measured by the LDVs was reduced to about 0.5 percent so that the LDV fluctuating signal to broad band noise level was typically of the order of 4:1. Furthermore, total head pitot-tube traverse measurements indicated a flat mean velocity profile with a boundary layer thickness of about 5 percent of the internal diameter of the measuring section. The oscillatory velocity profile measured by the LDVs was flat with negligible phase change up to the maximum radius which could be examined with the present viewing windows (that is to about half the distance to the walls). Acosta [1] has shown that under these conditions the oscillatory boundary layer yields a negligible effect on the oscillatory mass flow calculation.

(iii) Potential errors in the fluctuation measurements due to vibration of the components of the system were minimized by the heavy, rugged construction of the pump housing, volute and adjacent hydraulic components and by mounting the entire system on a very rigid support structure [22]. Originally the lasers and photomultipliers of the LDVs were mounted on a sturdy framework which was also rigidly attached to this mounting structure for the purpose of accurate measurement of the fluctuating velocities relative to the impeller. However, a number of preliminary tests established that more repeatable velocity measurements could be made by isolating the LDV framework from the main support structure so that the LDVs measured fluctuating velocity in laboratory coordinates. Then the required fluctuating velocities relative to the impeller were obtained by applying corrections derived from the outputs of two Statham accelerometers attached to the lucite window sections (see Appendix A). Normally these corrections were very small and did not exceed 5 percent of the fluctuating velocity in the worst case.

Other precautions and preliminary tests are described in Ng [22]. For example all the high points in the circuit were fitted with bleed valves for the collection and removal of air bubbles and the structural compliance of the hydraulic components between the measuring stations was minimized by the thick-walled steel construction of these components.

The six basic fluctuating signal measurements (two LDV, two pressure transducers and two accelerometer outputs) plus the basic reference signal exciting the system were simultaneously recorded in real time during the experiments. Subsequently each of the six measurements were cross-correlated with the reference signal using a Bafco return signal analyzer in order to obtain the in-phase and quadrature components of each signal at the

basic excitation frequency. No particular significance was attached to the phase relative to the reference signal; the purpose was to establish the phase between each of the six measurements.

As far as possible all of the electronic processing equipment used for each of the six measurements was calibrated dynamically ([22]) and these calibrations were then applied to the in-phase and quadrature components of the measurements. The intermediate results were six complex quantities \bar{v}_{M1} , \bar{v}_{M2} , \bar{P}_{M1} , \bar{P}_{M2} , \bar{a}_{M1} , and \bar{a}_{M2} representing the basic fluctuation measurements. Corrections for the accelerations and for the ancillary system dynamics were then applied as discussed in Appendix A. Transfer functions for the pump for each fluctuation frequency and mean operating state were then calculated as described in Appendix B.

Impellers and Their Steady State Performance

Experiments were performed with a number of 7.58 cm diameter axial flow impellers enclosed in a lucite housing to allow still and movie photography of the cavitation. Dynamic transfer functions were obtained for a simple 9° helical impeller and for an accurate scale model for the low pressure oxidizer turbopump in the Space Shuttle Main Engine (Impeller IV, Fig. 2). The former was made of stainless steel, the latter of aluminum which, incidentally, implied true scaling of the nondimensional static blade deflection under the applied hydrodynamic loads. With both impellers there were significant changes in the transfer function as the mean operating state, and in particular the cavitation number, was varied. Since these changes were similar in both impellers we shall for brevity confine our presentation to the results for the S.S.M.E. Impeller IV. It should however be noted that similar results for the helical inducer suggest that the transfer functions are at least qualitatively independent of the geometry of the inducer.

The impellers were driven at up to 12,000 rpm by a 15 kw motor. Considerable effort was expended to minimize the fluctuations in both the rotational speed and the axial motion of the impellers relative to the housing structure. These fluctuations were also monitored in order to insure that such extraneous motions did not impact the dynamic results. At low frequencies of excitation ($\Omega \approx 5 \text{ Hz}$) the rotational speed fluctuation measured using a proximity transducer and a 60 tooth steel wheel on

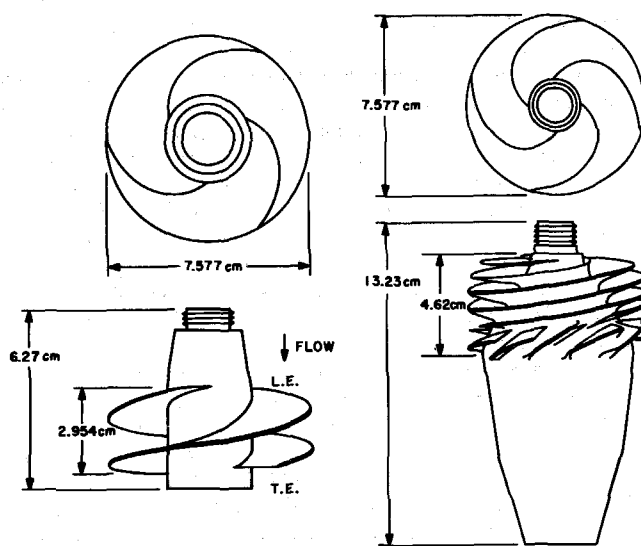


Fig. 2 Sketches of the two 7.58 cm diameter impellers tested. Impeller V on the left is a simple 9° helical inducer. Impeller IV on the right is 1/4 scale model of the low pressure oxidizer pump in the Space Shuttle Main Engine. (Simple ellipsoidal nose cones were added but are not shown.)

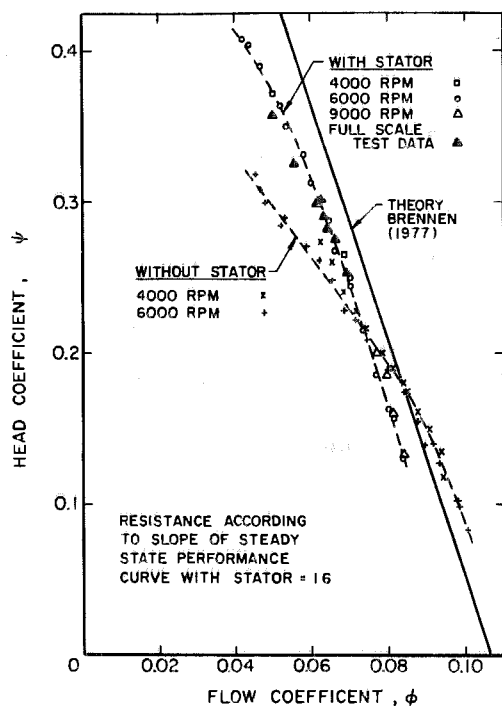


Fig. 3 Noncavitating performance of Impeller IV with and without the stator for various rotative speeds. Also shown are full-scale test data for this impeller (Rocketdyne Division, North American Rockwell, personal communication) and the theoretical, loss-less performance curve (Brennen (1977)).

the drive shaft was typically of the order of 0.1 percent; above $\Omega = 10$ Hz the level was too small to be measured, being less than 0.05 percent. Theoretical considerations [6] suggest that provided this level is much less than the percentage fluctuation in the cavitation number then it should have little effect on the dynamics; this was indeed the case in the present experiments.

Furthermore, measurements of the axial shaft motion with a proximity transducer indicated amplitudes less than 0.013 mm. under typical fluctuating conditions. Translated into an oscillatory velocity of the fluid relative to the impeller this implies a maximum 5 percent error in the measurement of the amplitude of an imposed 2 percent relative mass flow fluctuation at 40 Hz (based on a typical mean axial velocity of 25 cm/s). Though such an error is not entirely negligible, no attempt has been made to correct the results for this motion.

It was necessary to establish the steady state performance of the impellers under non-fluctuating conditions. The non-cavitating performance of Impeller IV, plotted as the head coefficient, ψ , versus the flow coefficient, ϕ , is presented in Fig. 3. Data with and without a stator similar to a candidate stator for the low pressure oxidizer turbopump on the S.S.M.E. is shown though only the performance with the stator is relevant to the present paper. Also shown are the full scale results with liquid oxygen (Rocketdyne Division, Rockwell International, personal communication); the agreement is excellent despite minor differences in the geometry of the pump discharge and volute. Comparison with a simple theoretical calculation which neglects friction and mixing losses [7] is also satisfactory.

The measured cavitation performance for Impeller IV is presented in Fig. 4 along with some preliminary full-scale data (Rocketdyne, COCA 1A tests, 740-015) for which $\phi = 0.069$. The points marked by letters in this figure are the mean operating points at which dynamic transfer functions were obtained.

During the course of the steady-state cavitating performance tests on the two inducers it was observed that strong, indeed violent, system oscillations could occur without any external excitation at certain flow coefficients, cavitation numbers and

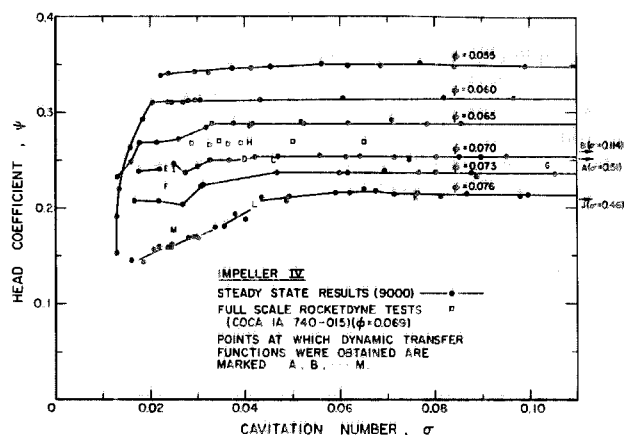


Fig. 4 Measured steady state cavitation performance for Impeller IV at 9000 rpm and various flow coefficients, ϕ , as indicated (—). Also shown are the results of some full scale tests for $\phi = 0.069$ performed by Rocketdyne (COCA 1A 740-015). The points at which dynamic transfer functions were obtained are shown by the letters; test A \rightarrow F were performed at 9000 rpm and $\phi = 0.070$; test G \rightarrow I at 12,000 rpm and $\phi = 0.070$; tests J \rightarrow M at 9000 rpm and $\phi = 0.076$.

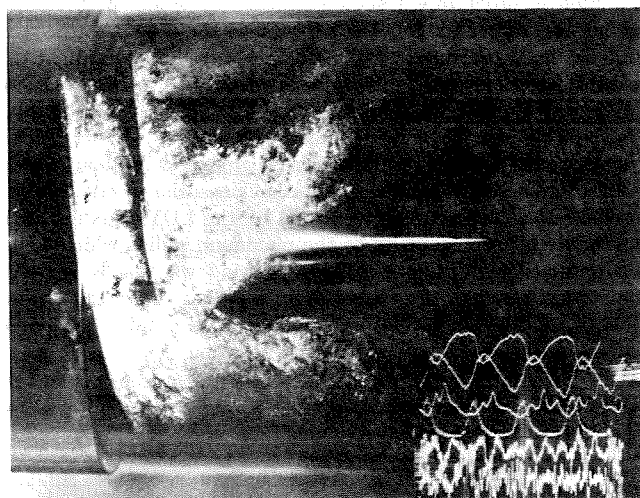


Fig. 5 High-speed still photograph of extensive cavitation on Impeller V during operation without external fluctuation at 9000 rpm, $\phi = 0.077$, $\sigma = 0.036$. The direction of flow is from right to left. At this operating point severe auto-oscillation at about 21 Hz was encountered. The inserted oscilloscope photograph shows the qualitative nature of the resulting oscillatory flow rates, pressures and accelerations; the flow rates are the upper two traces, the pressures the middle two and accelerations the last two with the upstream trace above the downstream trace.

rotative speeds. Oscilloscope traces indicating the form of the resulting large mass flow rate and pressure fluctuations for the helical impeller are shown in Fig. 5 superimposed on one high-speed still photograph showing that this condition occurred with extensive backflow cavitation. The particular instability frequency in this case was 21 Hz at 9000 rpm. Such auto-oscillation appears to be an important phenomenon ([29], [21], [33]) characteristic of cavitating inducers. Kamijo and Suzuki [13] and Kamijo, et al. [14] found that such low frequency system auto-oscillations (at about 10 Hz in their case) were preceded at higher cavitation numbers by a higher frequency (about 100 Hz) rotating or blade-to-blade oscillation of the cavitation. In general, however, heavy auto-oscillations appear to pose more of a threat to the integrity of impellers and to excitation of the hydraulic system. These phenomena are now under investigation in the present facility and the results will be reported at a later date. The transfer functions discussed here were obtained for mean operating conditions in which auto-oscillation did not

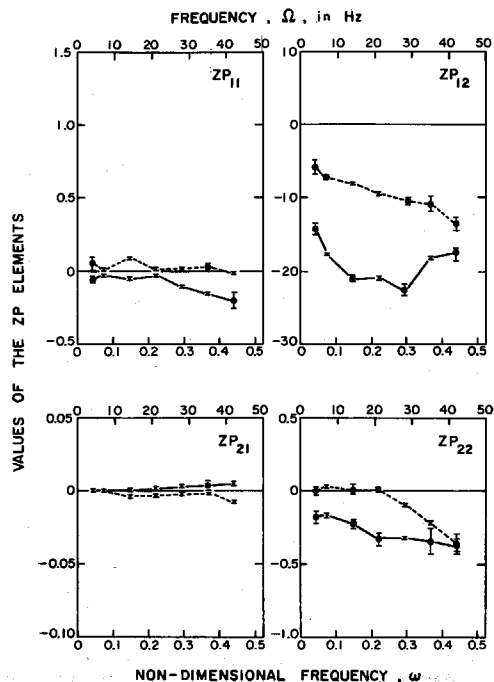


Fig. 6 The [ZP] transfer function for Impeller IV in the virtual absence of cavitation (point A, Fig. 4; $\psi = 0.25$, $\varphi = 0.070$, $\sigma = 0.51$, 9000 rpm). The real and imaginary parts of the elements (solid and dashed lines, respectively) are plotted against both the actual and the non-dimensional frequencies. The error bars are described in Appendix B.

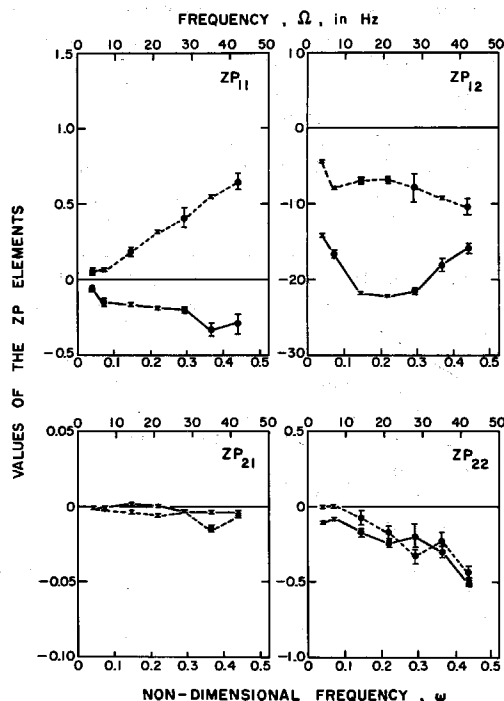


Fig. 7 The [ZP] transfer function for Impeller IV under conditions of moderate cavitation (point B, Fig. 4; $\psi = 0.26$, $\varphi = 0.70$, $\sigma = 0.114$, 9000 rpm). The extent and form of cavitation is seen in Fig. 9.

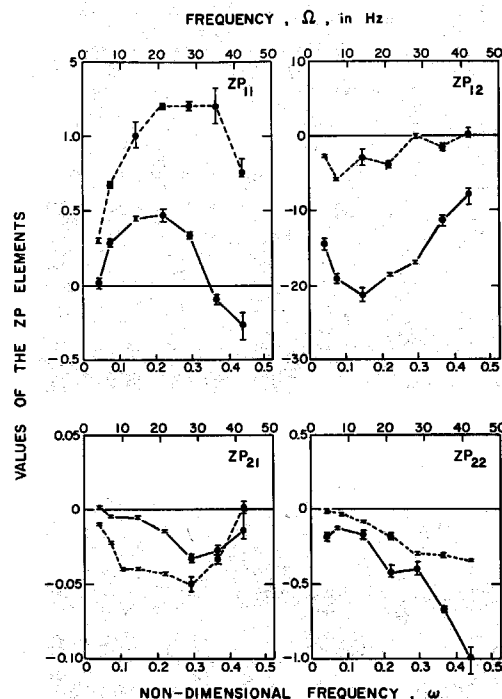


Fig. 8 The [ZP] transfer function for Impeller IV under conditions of extensive cavitation (point C, Fig. 4; $\psi = 0.25$, $\varphi = 0.70$, $\sigma = 0.046$, 9000 rpm). The extent and form of cavitation is seen in Fig. 9.

5 Experimental Transfer Matrices

Typical pump transfer matrices [ZP] for Impeller IV are shown in Figs. 6, 7, and 8 as functions of frequency; the real and imaginary parts of each of the four elements are shown as the solid and dashed lines respectively. The error bars represent the scatter manifest in the ZP elements due to the scatter in the original measurements of fluctuating pressure and mass flow rate (see Appendix B). It is much more difficult to estimate an overall uncertainty for these dynamic measurements and it is not unlikely that the presented error bars underestimate the possible error in the results.

The three transfer functions are for (i) a high "cavitation number" of 0.508 (Fig. 6) for which there was only a trace of tip vortex cavitation (ii) an intermediate σ of 0.114 (Fig. 6) at which substantial tip vortex, backflow and bubble cavitation could be observed (Fig. 9, upper photograph) and (iii) a low σ of 0.046 (Fig. 8) for which there was extensive cavitation (Fig. 9, lower photograph). These three mean operating states are indicated as A, B, C in Fig. 4 along with the other points (D, E, etc.) at which transfer matrices were obtained for Impeller IV. Most of these measurements were made at the design flow coefficient of $\varphi = 0.070$ and a rotative speed of 9000 rpm; however, some data was also obtained at $\varphi = 0.076$, 9000 rpm (points G \rightarrow I) and $\varphi = 0.070$, 12,000 rpm (points J \rightarrow M).

The significance of the system corrections which were applied (see Appendix A) in order to obtain these [ZP] transfer matrices is exemplified by comparison of Figs. 7 and 10, the latter being the [Z] transfer functions which would result in the absence of system corrections. The appropriate value of the downstream smoothing chamber compliance to be used in the system corrections was obtained by determining the value of C_2 which, for the noncavitating data, would make the final values of both ZP_{21} and ZP_{22} most nearly zero.

Before discussing the results it is worth repeating (see Section 3) that the very low cavitation number data (below about $\sigma = 0.04$) may contain significant nonlinearity due to the unavoidably large values in the magnitude of the fractional cavi-

occur. It seems likely that as the auto-oscillation regions are approached the dynamic transfer function for the pump undergoes changes which result in instability of the whole hydraulic system. An ongoing investigation is directed toward identifying those changes.

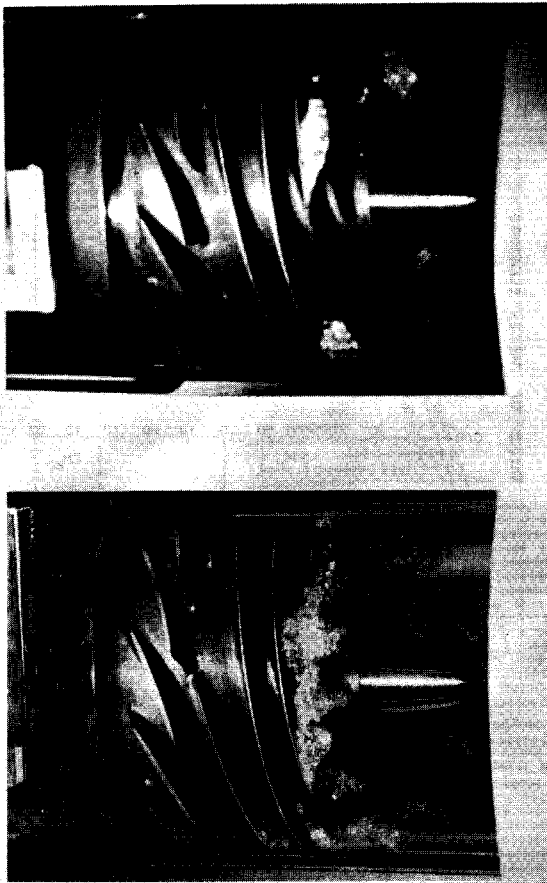


Fig. 9 High-speed still photographs of the cavitation on Impeller IV in conditions B (upper photograph) and C (lower photograph) of Fig. 4

tion number; this quantity reached values of the order of 0.7 at $\sigma \cong 0.024$. Furthermore one or two of the transfer matrices for Impeller IV were obtained for mean operating states in which the system was close to auto-oscillation (see Section 4); this was particularly the case for the point, E, (Fig. 4) at which some difficulty was encountered in obtaining data due to an incipient auto-oscillation which appeared to have a frequency in the neighborhood of 28-35 Hz.

To help in the interpretation of the transfer matrices it is convenient to recall the qualitative form of the matrices which result from some simple dynamic systems which have been used in the past as approximations to pump dynamics (eg. [27], [31]). For example the system comprising a cavitation compliance, K , followed by a resistance, R , and an inductance, L , yields

$$\begin{aligned} Z_{P11} &= j\omega KR - \omega^2 LK & ; & \quad Z_{P12} = -R - j\omega L \\ Z_{P21} &= -j\omega K & ; & \quad Z_{P22} = 0 \end{aligned}$$

If one further adds the effect of the change in volume of the cavitation due to the fluctuating angle of attack which results from the fluctuating inlet mass flow [6] this changes Z_{P22} to $-j\omega M$ and multiplies Z_{P12} by the factor $(1 - j\omega M)$ where M is termed the mass flow gain factor. The resulting determinant, D , is $(1 - j\omega M)$. The degree of validity of such a simple model is the kind of question the present program was intended to answer.

In the virtual absence of cavitation (Fig. 6) it appears that the pump dynamics are comprised of a simple impedance ($-Z_{P12}$) with no consistent non-zero values of the other three elements (the origin of the appreciable negative value of the real part of Z_{P22} in Fig. 6 is unknown; it did not appear consistently in other transfer functions); this is in accord with the conclusions one could reach based on simple ideas of continuity and insensitivity

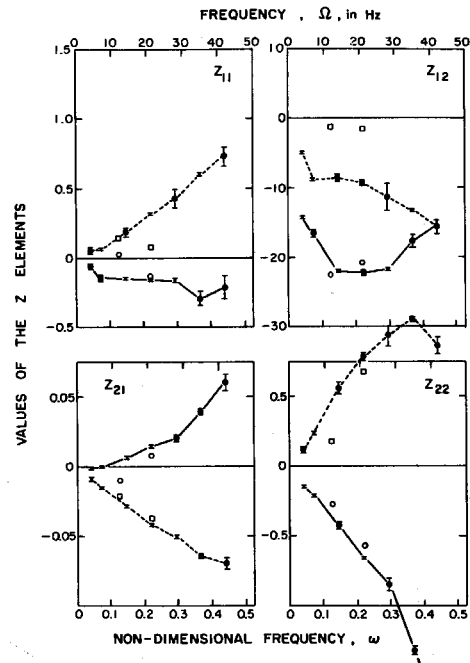


Fig. 10 The $[Z]$ transfer matrix prior to system corrections for Impeller IV under conditions of moderate cavitation (Point B, Fig. 4; $\psi = 0.26$, $\varphi = 0.070$, $\sigma = 0.114$, 9000 rpm). The extent and form of cavitation is seen in Fig. 9. The real and imaginary parts of the elements (solid and dashed lines respectively) are plotted against both the actual and nondimensional frequencies. Also shown are the real (O) and imaginary (□) parts of the transfer matrices for the third harmonic component of the fluctuations.

to the absolute pressure level. The impedance itself ($-Z_{P12}$) is however only very roughly like $(R + j\omega L)$. The quasi-steady resistance for Impeller IV based on the slope of Fig. 3 is about 16. The real part of $-Z_{P12}$ (we shall call this the "resistance" for convenience) does seem to approach a value of this order as ω tends to zero. However there was a consistent trend for the resistance to increase markedly at quite low frequencies and then level off to about 21 above about 14 Hz. Turning to the imaginary part of $-Z_{P12}$ (the inertive term) one can estimate analytically that the quasi-steady value of L is of the order of 60 for Impeller IV. While the slope of the imaginary part of $-Z_{P12}$ is not inconsistent with this value at the lowest frequencies there is a marked reduction in the magnitude of $\text{Imag}(-Z_{P12})$ at the higher frequencies. Both the increase in the resistance and the decrease in the inertance are trends which were also observed by Anderson, Blade and Stevens [3] in a centrifugal pump. Those authors suggested an explanation for these trends based on a more detailed impedance model with parallel resistance/inertance paths. A similar kind of model might have relevance in the present situation where the streamtubes near the hub would experience different dynamical effects from those near the tip. However it is also possible to envisage frequency dependent resistance arising from the complicated fluctuating boundary layers, separated flows and trailing vortex sheets associated with the inducer.

6 Transfer Matrices with Cavitation

Cavitation causes changes in all of the elements of the transfer function; these changes become appreciable at cavitation numbers much higher than that at which any degradation of steady state performance occurs. Referring to Figs. 7 and 8 as well as the other transfer matrices and looking first at Z_{P21} and Z_{P22} , it is apparent that the negative values of the imaginary parts of these quantities generally increase in magnitude as the frequency increases and thus suggest "compliance" and "mass flow gain factor" effects of the cavitation.



Fig. 9 High-speed still photographs of the cavitation on Impeller IV in conditions B (upper photograph) and C (lower photograph) of Fig. 4

tion number; this quantity reached values of the order of 0.7 at $\sigma \cong 0.024$. Furthermore one or two of the transfer matrices for Impeller IV were obtained for mean operating states in which the system was close to auto-oscillation (see Section 4); this was particularly the case for the point, E, (Fig. 4) at which some difficulty was encountered in obtaining data due to an incipient auto-oscillation which appeared to have a frequency in the neighborhood of 28-35 Hz.

To help in the interpretation of the transfer matrices it is convenient to recall the qualitative form of the matrices which result from some simple dynamic systems which have been used in the past as approximations to pump dynamics (eg. [27], [31]). For example the system comprising a cavitation compliance, K , followed by a resistance, R , and an inductance, L , yields

$$\begin{aligned} ZP_{11} &= j\omega KR - \omega^2 LK & ZP_{12} &= -R - j\omega L \\ ZP_{21} &= -j\omega K & ZP_{22} &= 0 \end{aligned}$$

If one further adds the effect of the change in volume of the cavitation due to the fluctuating angle of attack which results from the fluctuating inlet mass flow [6] this changes ZP_{22} to $-j\omega M$ and multiplies ZP_{12} by the factor $(1 - j\omega M)$ where M is termed the mass flow gain factor. The resulting determinant, D , is $(1 - j\omega M)$. The degree of validity of such a simple model is the kind of question the present program was intended to answer.

In the virtual absence of cavitation (Fig. 6) it appears that the pump dynamics are comprised of a simple impedance ($-ZP_{12}$) with no consistent non-zero values of the other three elements (the origin of the appreciable negative value of the real part of ZP_{22} in Fig. 6 is unknown; it did not appear consistently in other transfer functions); this is in accord with the conclusions one could reach based on simple ideas of continuity and insensitivity

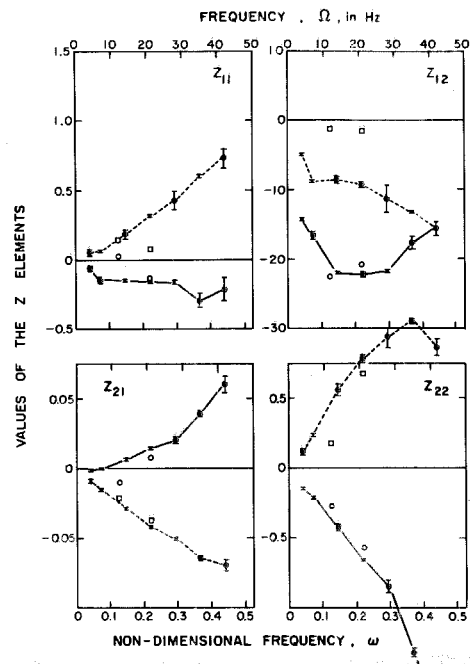


Fig. 10 The $[Z]$ transfer matrix prior to system corrections for Impeller IV under conditions of moderate cavitation (Point B, Fig. 4; $\psi = 0.26$, $\phi = 0.070$, $\sigma = 0.114$, 9000 rpm). The extent and form of cavitation is seen in Fig. 9. The real and imaginary parts of the elements (solid and dashed lines respectively) are plotted against both the actual and nondimensional frequencies. Also shown are the real (O) and imaginary (□) parts of the transfer matrices for the third harmonic component of the fluctuations.

to the absolute pressure level. The impedance itself ($-ZP_{12}$) is however only very roughly like $(R + j\omega L)$. The quasi-steady resistance for Impeller IV based on the slope of Fig. 3 is about 16. The real part of $-ZP_{12}$ (we shall call this the "resistance" for convenience) does seem to approach a value of this order as ω tends to zero. However there was a consistent trend for the resistance to increase markedly at quite low frequencies and then level off to about 21 above about 14 Hz. Turning to the imaginary part of $-ZP_{12}$ (the inertive term) one can estimate analytically that the quasi-steady value of L is of the order of 60 for Impeller IV. While the slope of the imaginary part of $-ZP_{12}$ is not inconsistent with this value at the lowest frequencies there is a marked reduction in the magnitude of $\text{Imag}(-ZP_{12})$ at the higher frequencies. Both the increase in the resistance and the decrease in the inertance are trends which were also observed by Anderson, Blade and Stevens [3] in a centrifugal pump. Those authors suggested an explanation for these trends based on a more detailed impedance model with parallel resistance/inertance paths. A similar kind of model might have relevance in the present situation where the streamtubes near the hub would experience different dynamical effects from those near the tip. However it is also possible to envisage frequency dependent resistance arising from the complicated fluctuating boundary layers, separated flows and trailing vortex sheets associated with the inducer.

6 Transfer Matrices with Cavitation

Cavitation causes changes in all of the elements of the transfer function; these changes become appreciable at cavitation numbers much higher than that at which any degradation of steady state performance occurs. Referring to Figs. 7 and 8 as well as the other transfer matrices and looking first at ZP_{21} and ZP_{22} , it is apparent that the negative values of the imaginary parts of these quantities generally increase in magnitude as the frequency increases and thus suggest "compliance" and "mass flow gain factor" effects of the cavitation.

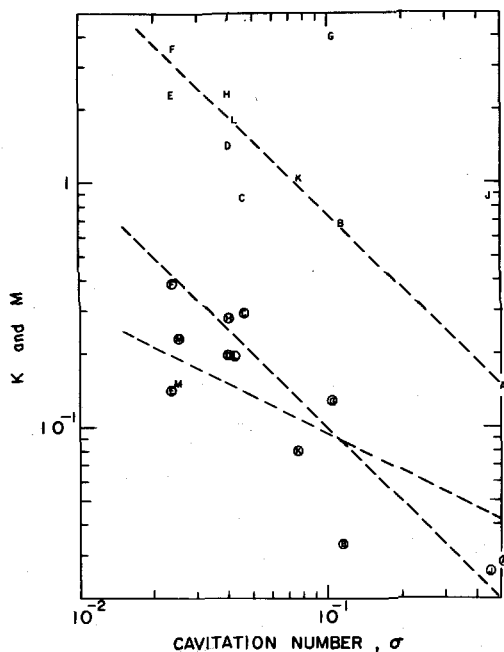


Fig. 11 Estimated values of the "compliance," K , (circled letters) and "mass flow gain factor," M , (uncircled letters) from the dynamic transfer functions for Impeller IV as functions of the cavitation number. The dashed lines are suggested trends with slopes of σ^{-1} and $\sigma^{-1/2}$.

In order to examine the low frequency content of these quantities the imaginary parts of ZP_{21} and ZP_{22} were fitted by a least squares procedure to a functional form, $-j\omega A + j\omega^2 B$, where A and B are the fitted quantities. The resulting "compliances," K (A for ZP_{21}) and "mass flow gain factors," M (A for ZP_{22}) are plotted in Fig. 11 against cavitation number, σ . Though there is significant scatter it is clear that both K and M increase with the extent of cavitation; the dependence on σ is of the order of $\sigma^{-1/2}$ to σ^{-1} . Brennen and Acosta [6] evaluated the theoretical K and M which would result from attached blade cavities alone at low frequencies. The experimental values of Fig. 11 are substantially larger than those theoretical predictions for blade cavities. However the photographs (for example, Fig. 9) show larger volumes of bubbly cavitation. Some previous theoretical estimates [4] indicated that such cavitation typically yields values of K which are proportional to $\sigma^{-1/2}$.

It should however be emphasized that the effects of cavitation on ZP_{21} , ZP_{22} manifest in the transfer matrices are clearly more complex than those of a simple compliance and mass flow gain factor. The imaginary parts are not linear with frequency, and though the real part of ZP_{21} did not exhibit any consistent trend and was always fairly small, the real part of ZP_{22} consistently had negative values increasing in what seemed to be a quadratic manner with increasing frequency; the "coefficient" appeared to increase with decreasing σ .

Reduction in σ also caused progressive changes in the impedance element, ZP_{12} . Though the resistance remained close to its non-cavitating value at low frequencies (a small increase is suggested by the present data) the resistance became significantly smaller at the higher frequencies and indeed could change sign at the highest frequencies and smallest σ . Finally the real part of ZP_{11} exhibited increasingly positive values at low frequency and increasing negative values at high frequency and the imaginary part exhibited increasingly large positive values with frequency and σ . This behavior of ZP_{11} would be crudely consistent with the simple model above if a pressure gain component or pressure amplifier were inserted in the model, though the change in the real part to negative values at higher frequencies would not be forthcoming from such a model.

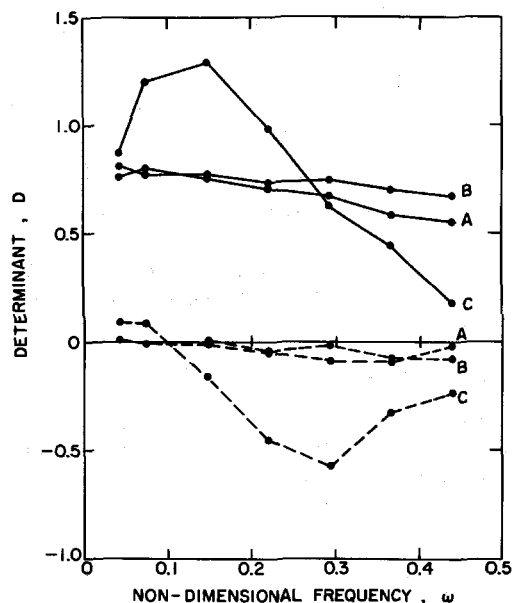


Fig. 12 The determinant, D , for the transfer functions of Figs. 6, 7, and 8 as a function of frequency. Solid and dashed lines are used for the real and imaginary parts respectively. The scatter on this data derived from the error bars of Figs. 6, 7, and 8 is ± 0.1 in the worst case.

An interesting sidelight on the dynamic results was provided by the observation that the slotted cylinder design of the fluctuator was such that the resulting hydraulic oscillations contained an observable third harmonic. The return signal analyzer had the capability of measuring these third harmonic components and the question naturally arose as to whether the pump transfer function for the third harmonic was similar to that for the fundamental. Though the accuracy of these third harmonic measurements is considerably poorer than those of the fundamental due to the much lower signal levels a typical result is displayed in Fig. 10; the agreement is probably as good as could be expected.

Values of the determinant, D , of $[ZP] + [I]$ where $[I]$ is the unit matrix were also computed for all the transfer matrices. For a purely passive dynamical system the value of this should be unity due to the theorem of reciprocity. Thus the actual value represents some measure of the active dynamical component in the pump transfer function. (It should be noted that this determinant is independent of the system corrections of Appendix A.) The values for the transfer matrices of Figs. 6, 7, and 8 are presented in Fig. 12. These, and values from the other transfer matrices, strongly suggest that D is predominantly real and nearly independent of ω for the noncavitating operating states. Furthermore its value ranged between about 0.75 and 1.0. Thus without cavitation, it is fairly close to a passive system. On the other hand as the cavitation number was decreased both the real and imaginary parts changed in a manner typified by the results for the point C. Clearly the system is no longer passive and such a trend may result in phenomena such as auto-oscillation in which the pump deposits a portion of its mean inflow of energy into flow fluctuations.

7 Concluding Remarks

In this paper we have described experiments designed to measure the dynamic transfer functions for cavitating (and non-cavitating) hydraulic machines as functions of frequency and mean operating state. We have also presented and discussed the measured transfer functions for one particular axial inducer. Though some of the characteristics of these transfer functions do conform roughly to existing simple theories, it is also true,

particularly in the cavitating cases, that major effects seen in the results remain to be explained theoretically. We intend to present some further theoretical models in the near future.

There are also further detailed questions about the dynamics which need further experimental investigation; the scaling of the dynamics to geometrically similar machines of different size requires further research; the thermal effects on cavitation in nominally steady flows is well-known and clearly there may be analogous effects on the dynamics; the phenomena of rotating cavitation and auto-oscillation require further study. It is hoped that experiments in the future will begin to resolve some of these questions.

Acknowledgments

The authors wish to express their sincere thanks to Professor Allan Acosta for his help and encouragement; we also owe a debt of gratitude to Dr. Sheldon Rubin, Jim Fenwick, Loren Gross and especially to David Braisted and undergraduates Javier DelValle, Siu Cheung, Robert Higley and Philip Engelauf who worked on the experiments. This work was supported by NASA George Marshall Space Flight Center under contracts NAS 8-29313 and NAS 8-28046.

APPENDIX A

Acceleration and System Corrections

Following the application of the dynamic calibrations of the electronic processing equipment, complex dimensional values were obtained for the fluctuating pressures, \tilde{P}_{M1} and \tilde{P}_{M2} , velocities, \tilde{v}_{M1} and \tilde{v}_{M2} , and accelerations \tilde{a}_{M1} and \tilde{a}_{M2} (the subscripts 1 and 2 are used for inlet and discharge quantities, respectively). The positions of each of these measurements are indicated in Fig. A1.

The purpose of this appendix is to indicate how this data was utilized to obtain the equivalent fluctuating total pressures and mass flow rates relative to an impeller and system which is *not* moving structurally with accelerations \tilde{a}_{M1} and \tilde{a}_{M2} .

The fluid velocities relative to the impeller are $\tilde{v}_{M1} + j\tilde{a}_{M1}/\Omega$, $\tilde{v}_{M2} + j\tilde{a}_{M2}/\Omega$ and these are converted to the non-dimensional relative mass flows \tilde{m}_{N1} , \tilde{m}_{N2} (see Section 1) by multiplying by $A_{BB}/A_{II}U_T$ where A_{BB} is the flow area at the measurement station cross-section. The quantities \tilde{m}_{N1} , \tilde{m}_{N2} then pertain to the mass flow rates at the LDV viewing windows (BB and DD of Fig. A1).

The pressure signals include an acceleration head due to the vibration which is most conveniently removed by relating them to the same reference origin in the oscillating system. The chosen origin is the leading edge of the impeller blades so that the nondimensional pressures \tilde{p}_{N1} and \tilde{p}_{N2} where

$$\tilde{p}_{N1} = (\tilde{P}_{M1} - \rho l_1 \tilde{a}_{M1}) / \left(\frac{1}{2} \rho U_T^2 \right) \quad (A1)$$

$$\tilde{p}_{N2} = (\tilde{P}_{M2} + \rho l_2 \tilde{a}_{M1} + \rho l_3 \tilde{a}_{M2}) / \left(\frac{1}{2} \rho U_T^2 \right) \quad (A2)$$

are those which would effectively occur at the pressure measurement stations in the absence of the structural translational vibration; the lengths l_1 , l_2 , and l_3 are indicated in Fig. A1. It should be stressed that though these acceleration corrections are essential for proper reduction of the data, the structural rigidity of the entire system was such that the corrections are rather small; for example the effect on the fluctuating mass flow rates was normally less than 5 percent.

Transfer matrices, denoted by $[Z]$, could then be obtained by utilizing \tilde{p}_{N1} , \tilde{m}_{N1} , \tilde{p}_{N2} , and \tilde{m}_{N2} . But such transfer functions would apply to all of the flow between the sections AA and CC

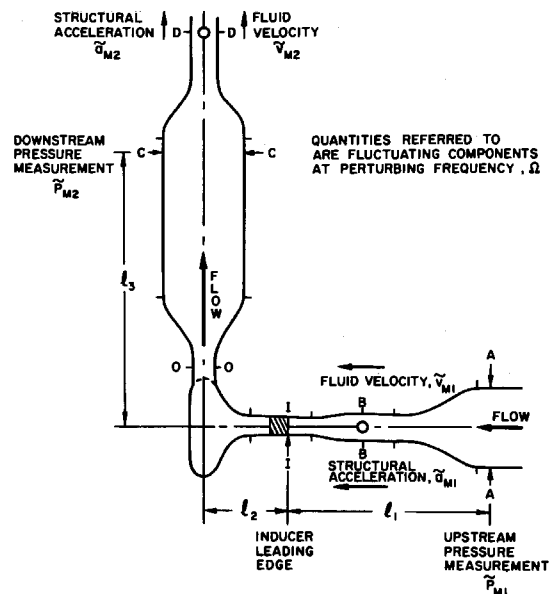


Fig. A1 Schematic of measurement stations on the dynamic pump test facility

of Fig. A1 and would therefore include the dynamics of portions of the inlet and discharge lines as well as the pump itself. In order to more clearly isolate the transfer function of the pump, we shall rather arbitrarily define the pump as extending from the inlet plane at the leading edge of the blades, II, and the plane, OO, at discharge from the volute. The volute is included because we cannot with any confidence predict the dynamics of the flow therein. Fluctuating quantities calculated for the inlet plane, II, (Fig. A1) and the discharge plane, OO, will be denoted by the single subscripts 1 and 2, respectively.

As described in the introduction the intent is to define the transfer function for the pump in terms of total pressure quantities \tilde{h}_1 and \tilde{h}_2 and the mass flow rates \tilde{m}_1 and \tilde{m}_2 which must now be obtained from \tilde{p}_{N1} , \tilde{p}_{N2} , \tilde{m}_{N1} , \tilde{m}_{N2} . Dealing first with the inlet quantities theoretical estimates indicated that (i) the structural and liquid compliance between BB and II was negligible and (ii) the impedance between AA and II would to all intents and purposes consist only of an inertance, \mathcal{L}_1 , of dimensional magnitude 70 m^{-1} (the dimensionless inertance is then, $L_1 = 2\mathcal{L}_1 A_{II}/H$). It follows that

$$\tilde{m}_1 = \tilde{m}_{N1} \quad (A3)$$

$$\tilde{h}_1 = \tilde{p}_{N1} - j\omega L_1 \tilde{m}_1 + 2\varphi \left(\frac{A_{II}}{A_{AA}} \right)^2 \tilde{m}_1 \quad (A4)$$

where A_{AA} is the cross-sectional area of the flow at AA; the last term was always negligible.

The downstream dynamics are more complicated because of the smoothing section. A theoretical evaluation of the inertance between OO and CC indicated a value $\mathcal{L}_2 = 20.6 \text{ m}^{-1}$ ($L_2 = 2\mathcal{L}_2 A_{II}/H$). Due to the flow smoothing elements the impedance also includes a resistance whose static value was measured as $108.8 \text{ m}^{-1} \text{ s}^{-1}$ (the nondimensional quantity is obtained by multiplication by $2A_{II}/U_T$). Finally the size of the downstream smoothing section and the large amount of fluid it contains means that the section from OO to DD has a significant structural and liquid compliance, whose nondimensional value will be denoted by C_2 . Thus

$$\tilde{m}_2 = \tilde{m}_{N2} + j\omega C_2 \left\{ \tilde{P}_{M2} / \left(\frac{1}{2} \rho U_T^2 \right) \right\} \quad (A5)$$

$$\tilde{h}_2 = p_{N2} + 2\varphi \left(\frac{A_{II}}{A_{CC}} \right)^2 \tilde{m}_2 + (j\omega L_2 + R_2) \tilde{m}_2 \quad (A6)$$

where A_{CC} is the cross-sectional area at CC .

All of these system corrections have small effects in the transfer function results with the exception of the terms involving C_2 . Theoretical estimates indicated that the structural and liquid compressibility contributions to C_2 would have dimensional values of 2.04×10^{-8} and $2.35 \times 10^{-8} \text{ m}^2$ respectively; the sum would be multiplied by $U_T^2/2HA_{II}$ to obtain the dimensionless C_2 . But since the structural and liquid compliance in the rest of the system between AA and CC is many times smaller than $4.39 \times 10^{-8} \text{ m}^2$, the latter could be checked during measurements of the transfer functions under noncavitating conditions. The value of C_2 derived from such tests was about 50 percent greater than the theoretical estimate; this experimental value was thereafter employed for the system corrections to the cavitating results. Finally the pump transfer matrices, denoted by $[ZP]$, were computed from $\tilde{h}_1, \tilde{h}_2, \tilde{m}_1, \tilde{m}_2$ in the manner described in Appendix B.

APPENDIX B

Transfer Function Computation

As discussed in Section 2 three or four linearly independent "sets" of data were obtained for each frequency and mean operating state; we shall denote the number of sets by K . Furthermore, each measurement of $\tilde{h}_1, \tilde{h}_2, \tilde{m}_1$, and \tilde{m}_2 was repeated at least four times. The differences between these repeated measurements represents some measure of the scatter or uncertainty in the data. We denote this number of individual measurements of each quantity for each set by L .

Thus the total data package for each mean operating condition and frequency was comprised of $L \times K$ arrays of values denoted by a superscript:

$$\{\tilde{h}_1^n, \tilde{h}_2^n, \tilde{m}_1^n, \tilde{m}_2^n\} \quad \text{for } n = l + L(k - 1) \\ l = 1, \dots, L \quad (B1) \\ k = 1, \dots, K.$$

The following method was used to obtain the matrix $[ZP]$ which best fitted the data

$$\begin{bmatrix} ZP_{11} + 1 & ZP_{12} \\ ZP_{21} & ZP_{22} + 1 \end{bmatrix} = S_8 \begin{bmatrix} S_2 S_5 - S_3 S_6 & S_1 S_6 - S_2 S_8 \\ S_4 S_5 - S_9 S_7 & S_1 S_7 - S_4 S_3 \end{bmatrix} \quad (B2)$$

where an overbar denotes the complex conjugate and

$$S_1 = \sum_{i=1}^I \tilde{h}_1^i \bar{p}_1^i \quad S_2 = \sum_{i=1}^I \tilde{h}_2^i \bar{h}_1^i \quad S_3 = \sum_{i=1}^I \tilde{m}_1^i \bar{h}_1^i \\ S_4 = \sum_{i=1}^I \tilde{m}_2^i \bar{h}_1^i \quad S_5 = \sum_{i=1}^I \tilde{m}_1^i \bar{m}_1^i \quad S_6 = \sum_{i=1}^I \tilde{h}_2^i \bar{m}_1^i \quad (B3) \\ S_7 = \sum_{i=1}^I \tilde{m}_2^i \bar{m}_1^i \quad S_8 = (S_2 S_5 - S_3 S_6)^{-1}.$$

This minimizes the sum of the squares of the spectral radii of the residues in the two equations comprising the transfer function equation.

For the overall best fit, i is identical to n in (B1) and $I = K \times L$. However, the same procedure was also used to examine how the uncertainties in the original data manifest themselves as uncertainties in the matrix $[ZP]$. The error bars in the Figs. 11, 12, 13, 14 were obtained by calculating a series of transfer functions $[ZP]$, $l = 1, \dots, L$ with $i = 1, \dots, K$ and $I = K$.

Though they will not be presented here other subsets of the data array were also investigated in order to determine, for example, the influence of individual sets and the linear independence of the sets.

References

- Acosta, A. J., "An Experimental Study of Cavitating Inducers," *Proc. of Second O. N. R. Symposium on Naval Hydrodynamics*, Aug. 25-29, 1958, (ACR-38).
- Acosta, A. J., "Unsteady Effects in Flow Rate Measurement of the Entrance of a Pipe," *ASME J. Fluids Eng.*, Vol. 98, No. 3, 1976, pp. 562-563.
- Anderson, D. A., Blade, R. J., and Stevens, W., "Response of a Radial-Bladed Centrifugal Pump to Sinusoidal Disturbances for Non-Cavitating Flow," NASA, TN D-6556, 1971.
- Brennen, C., "The Dynamic Behavior and Compliance of a Stream of Cavitating Bubbles," *ASME JOURNAL OF FLUIDS ENGINEERING*, Vol. 95, No. 4, 1973, pp. 533-542.
- Brennen, C., and Acosta, A. J., "Theoretical, Quasi-Static Analysis of Cavitation Compliance in Turbopumps," *Journal of Spacecraft and Rockets*, Vol. 10, No. 3, 1973, pp. 175-180.
- Brennen, C., and Acosta, A. J., "The Dynamic Transfer Function for a Cavitating Inducer," *ASME JOURNAL OF FLUIDS ENGINEERING*, Vol. 98, 1976, pp. 182-191.
- Brennen, C., "On Non-Cavitating Axial Inducer Performance," A brief, technical note in preparation, 1977.
- Fanelli, M., "Further Considerations on the Dynamic Behavior of Hydraulic Turbo-Machinery," *Water Power*, June 1972, pp. 208-222.
- Farrel, E. C., and Fenwick, J. R., "Pogo Instabilities Suppression Evaluation," NASA Report CR-134500, 1973.
- Ghahremani, F. G., "Turbopump Cavitation Compliance Report No. TOR-0059(6531-01)-2, Aerospace Corporation, El Segundo, Calif., 1970.
- Gibbs, K. P., and Oliver, A. G., "Special Requirements for Pumps for Sodium Cooled Fast Reactors," Pumps for Nuclear Power Plant, Convention sponsored by the Fluid Machinery and Nuclear Power Plant Groups of the Institute of Mechanical Engineers, University of Bath, April 22-25, 1973, pp. 119-124.
- Jaeger, C., "The Theory of Resonance in Hydro-Power Systems, Discussion of Incidents and Accidents Occurring in Pressure Systems," *ASME Journal of Basic Engineering*, Vol. 85, 1973, pp. 631-640.
- Kamijyo, K., and Suzuki, A., "An Experimental Investigation of Flat-Plate Helical Inducers for Rocket Turbopumps," Nat. Aerospace Lab. (Japan), N. A. L. Rept. TR-345, 1973.
- Kamijyo, K., Suzuki, A., Shimura, T., Hashimoto, R., Watanabe, M., Watanabe, Y., Iwabuchi, T., and Mori, Y., "Experimental Investigation of Small, High-Speed, High-Head Liquid Oxygen Pump," Nat. Aerospace Lab. (Japan), N. A. L. Rept. TR-415, 1975.
- Kim, J. H., and Acosta, A. J., "Unsteady Flow in Cavitating Turbopump," *JOURNAL OF FLUIDS ENGINEERING*, Vol. 97, 1975, pp. 412-417.
- Knapp, R. T., "Complete Characteristics of Centrifugal Pumps and Their Use in the Prediction of Transient Behavior," *TRANS. ASME*, Nov. 1937, pp. 683-689.
- Liao, G. S., "Protection of Boiler Feed Pump Against Transient Suction Decay," *ASME Journal of Engineering for Power*, Vol. 96, 1974, pp. 247-255.
- Liao, G. S., and Leung, P., "Analysis of Feedwater Pump Suction Pressure Decay Under Instant Turbine Load Rejection," *ASME Journal of Engineering for Power*, Vol. 94, 1972, pp. 83-90.
- Lock, M., and Rubin, S., "Passive Suppression of POGO on the Space Shuttle," NASA Rept. CR-132452, 1974.
- NASA, "Prevention of Coupled Structure-Propulsion Instability," NASA Rept. SP-8055, 1970.
- Natanzon, M. S., Bl'tsev, N. I., Bazhanov, V. V., and Leydervarger, M. R., "Experimental Investigation of Cavitation-Induced Oscillations of Helical Inducers," *Fluid Mechanics, Soviet Res.*, Vol. 3, No. 1, 1974, pp. 38-45.
- Ng, S. L., "Dynamic Response of Cavitating Turbomachines," PhD thesis, California Institute of Technology, Pasadena, Calif., (Rept. E 184.1, Div. of Eng. and Appl. Sci., C.I.T., Aug. 1976).
- Ng, S. L., Brennen, C., and Acosta, A. J., "The Dynamics of Cavitating Inducer Pumps," *Proc. Int'l. Conf. on Two Phase Flow and Cavitation*, Int'l. Assoc. Hyd. Res., Grenoble, 1976.
- Norquist, L. W. S., Marcus, J. P., and Ruscio, D. A., "Development of Close-Coupled Accumulators for Suppressing Missile Longitudinal Oscillations (POGO)," AIAA 5th Propulsion Joint Specialist Conference, AIAA Paper No. 69-547, 1969.
- Rocketdyne Rept., "Investigation of 17-Hz, Closed-Loop

Instability on S-II Stage of Saturn V," Rocketdyne Div., Rockwell Int'l, Rept. No. R-7970, 1969.

26 Rocketdyne, "Test Results of SSME Low Pressure Oxidizer Turbopump Model Inducer," Internal letter No. R/H 4194-3074, 1974.

27 Rubin, S., "Longitudinal Instability of Liquid Rockets Due to Propulsion Feedback (POGO)," *J. Spacecraft and Rockets*, Vol. 3, No. 8, 1966, pp. 1188-1195.

28 Rubin, S., Wagner, R. G., and Payne, J. G., "POGO Suppression on Space Shuttle—Early Studies," NASA Rept. CR-2210, 1973.

29 Sack, L. E., and Nottage, H. B., "System Oscillations Associated With Cavitating Inducers," *ASME J. Basic Engr.*, Vol.

87, No. 4, 1965, pp. 917-925.

30 Streeter, V. L., and Wylie, E. B., *Hydraulic Transients*, McGraw-Hill, New York, 1967.

31 Vaage, R. D., Fidler, L. E., and Zehnle, R. A., "Investigation of Characteristics of Feed System Instabilities," Final Rept. MCR-72-107, Martin Marietta Corp., Denver, Colo., 1972.

32 Wagner, R. G., "Titan II Engine Transfer Function Test Results," Report No. TOR-0059 (G471)-9, Aerospace Corp., El Segundo, Calif., 1971.

33 Young, W. E., Murphy, R., and Reddecliff, J. M., "Study of Cavitating Inducer Instabilities," Pratt and Whitney Aircraft, Florida Research and Development Center, Rept. PWA FR-5131, 31st Aug. 1972.

CALL FOR PAPERS

2ND SYMPOSIUM ON TURBULENT SHEAR FLOWS

July 2-4, 1979
Imperial College
London, England

AIM. To advance the understanding of physical phenomena and existing capabilities for calculating turbulent shear flows. Discussion in line with these aims will be initiated by the presentation of technical papers and scheduled and impromptu debates.

SCOPE. The symposium will allow the presentation of the latest developments in the calculation of flow and heat transfer properties in turbulent shear flows. The improvement of the physical understanding of turbulent shear flows and related measurements are considered essential to the advancement of calculational methods and will be included in the symposium.

SESSIONS: Approximately 15 formal sessions are planned. Contributions are welcomed from the following general areas.

Fundamentals	New theories and concepts or measurements that illuminate the nature of turbulence
Turbulence Models	New developments within the framework of classical single- or two-point closures
Heat and Pollutant Transport	Particular emphasis on the physics of scalar transport by turbulence whether passive or coupled through buoyancy or other agents
Combustion	Physical aspects of turbulence effects on pre-mixed and diffusion flames
Numerical Schemes	New and improved numerical methods for calculating turbulent flows
Applications	Turbulent flow calculation schemes applied to problems of engineering importance

ABSTRACTS. Papers will be selected based upon extended abstracts, in English, of about 1000 words in length. The abstracts, typed double spaced, should state clearly the purpose, results and conclusions with supporting figures as appropriate. All reference to units and dimensions should be in SI units. Five copies of the abstracts should be submitted.

PUBLICATION. Those authors whose abstracts have been accepted will be required to supply a manuscript typed on mats and acceptable for reproduction. Bound copies of all papers will be presented to those attending the symposium.

DEADLINES. Final date for submission of abstracts —August 31, 1978
Authors informed of acceptance or rejection —Dec. 31, 1978
Final date for submission of typed manuscripts —March 31, 1979

Send abstracts to:

Professor F. W. Schmidt
Department of Mechanical Engineering
The Pennsylvania State University
University Park, Pa. 16802, U.S.A.